Time-Varying Formation Control for Heterogeneous Planar Underactuated Multivehicle Systems

Bo Wang
Department of Mechanical Engineering,
Center for Nonlinear Dynamics and Control (CENDAC),
Villanova University,
Villanova, PA 19085
e-mail: bwang6@villanova.edu

Sergey G. Nersesov
Department of Mechanical Engineering,
Center for Nonlinear Dynamics and Control (CENDAC),
Villanova University,
Villanova, PA 19085
e-mail: sergey.nersesov@villanova.edu

Hashem Ashrafiuon[1]
Department of Mechanical Engineering,
Center for Nonlinear Dynamics and Control (CENDAC),
Villanova University,
Villanova, PA 19085
e-mail: hashem.ashrafiuon@villanova.edu

This paper presents a distributed control approach for time-varying formation of heterogeneous planar underactuated vehicle networks without global position measurements. All vehicles in the network are modeled as generic three degree-of-freedom planar rigid bodies with two control inputs, and are allowed to have nonidentical dynamics. Feasible trajectories are generated for each vehicle using the nonholonomic constraints of the vehicle dynamics. By exploiting the cascaded structure of the planar vehicle model, a transformation is introduced to define the reduced order error dynamics, and then, a sliding-mode control law is proposed. Low-level controller for each vehicle is derived such that it only requires relative position and local motion information of its neighbors in a given directed communication network. The proposed formation control law guarantees the uniform global asymptotic stability (UGAS) of the closed-loop system subject to bounded uncertainties and disturbances. The proposed approach can be applied to underactuated vehicle networks consisting of mobile robots, surface vessels, and planar aircraft. Simulations are presented to demonstrate the effectiveness of the proposed control scheme. [DOI: 10.1115/1.4053359]

1 Introduction

1.1 Motivation and Literature Review. Control of planar underactuated vehicles has been a very active research area due to its intrinsic nonlinear nature and widely practical applications. Nonholonomicity and underactuation are two main obstacles in control design of planar underactuated vehicles. Specific control approaches have been proposed for nonholonomic mobile robots [1–3], underactuated surface vessels [4,5], and planar vertical takeoff and landing (PVTOL) aircraft [6,7] based on the specific structures of their dynamics. In the authors' previous work [8], a trajectory tracking control framework was proposed for generic planar underactuated vehicles that can be applied to various forms of planar underactuated vehicles, including wheeled mobile robots, marine surface vessels, and PVTOL aircraft. The motivation for this work is to develop a cooperative control algorithm that can be applied to networks, which include these diverse types of vehicles. Application examples include networks consisting of ground vehicles and surface vessels with on-board robotic manipulators cooperatively handling loads in canals and for surveillance operations where coordination between the units in the river and on the ground is needed.

Research on cooperative control of vehicle networks has grown overwhelmingly over the past several years since it has many applications in practice such as search and rescue, reconnaissance, and surveillance, to name a few [9]. Leader–follower formation control is a natural extension of the classical trajectory tracking control problem to the multi-agent systems, and it is particularly appreciated in many applications for its simplicity and scalability [10]. In Ref. [11], a virtual leader coordination strategy has been proposed for multi-agent formation control. The virtual leader tracks its reference trajectory, while the agents maintain the desired formation at the same time. The motion feasibility problem for multi-agent formations has been studied in Ref. [12], where algebraic conditions were developed to determine the feasibility of the formation motion based on the kinematics model of agents. Various consensus and formation control approaches were proposed in the literature for vehicles modeled as single and double integrators [13–15], linear systems [16], fully actuated rigid body attitude dynamics [17,18], and fully actuated Euler-Lagrangian systems [19]. For underactuated multivehicle networks, several cooperative control methods have been developed in the literature according to different models of vehicles. Leader–follower formation control of multiple nonholonomic mobile robots was considered in Refs. [10,20–25]. We refer the readers to the survey paper [26] for a comprehensive literature review of formation control of ground vehicles. Leader–follower cooperative control of multiple underactuated surface vessels was considered in Refs. [27–29], and cooperative control of underactuated aircraft was considered in Refs. [30–32]. While this brief discussion is not intended to be a comprehensive review, it is found that although most of control strategies in the existing work can successfully be applied to *homogeneous* underactuated multivehicle networks, these control designs heavily depend on the specific structures of vehicle dynamics and hence can hardly be applied to control *heterogeneous* networks of underactuated vehicles. In practice, however, it is useful if a group of vehicles can cooperate with each other regardless of the model parameters or even structures of their dynamic models. Only a few works discuss the formation control problem of *heterogeneous underactuated* networks. In Ref. [33], a formation stabilization control law has been proposed for heterogeneous underactuated mechanical systems using a passivity-based control technique and applied to formation stabilization of PVTOL aircraft. Using a similar passivity-based control idea, a cooperative control law has been proposed in Ref. [34] for formation tracking of heterogeneous planar underactuated vehicles. These methods, however, require global position measurements for feedback purposes.

In the survey paper [35], multi-agent formation control strategies were reviewed and categorized into position-, displacement- and distance-based approaches depending on the sensing capability and the interaction topology. In the position-based approach, such as in Refs. [21], [27], and [28], agents sense their positions with respect to a global coordinate system, and interactions are

[1]Corresponding author.

Contributed by the Dynamic Systems Division of ASME for publication in the Journal of Dynamic Systems, Measurement, and Control. Manuscript received June 17, 2021; final manuscript received December 18, 2021; published online January 25, 2022. Assoc. Editor: Luca Consolini.

not necessarily required because the desired formation can be achieved by position control of individual agents. Distance-based coordination approaches, such as Ref. [36], do not need the local coordinate systems to be aligned with each other, but the interaction graph has to be rigid or persistent and must contain redundant connections. The displacement-based approach balances the sensing capability and the interaction requirements, and thus, is particularly useful in applications where the GPS signal is not available while onboard sensors can provide measurements necessary for feedback. In the displacement-based approach, the desired formation is specified by the interagent positions, which implies that agents need to know their orientation in the global coordinate system.

In this work, we employ a displacement-based approach for coordinated motion and apply it to formation control of networks of heterogeneous underactuated vehicles. Moreover, we allow for the *time-varying* geometric pattern of the vehicles to capture the changes in vehicle arrangements as well as obstacle and collision avoidance. To the best of our knowledge, a rigorous distributed displacement-based control law that can be applied to time-varying formation of *heterogeneous* underactuated vehicle networks has not yet been developed. The preliminary results of this research were presented in Ref. [37].

1.2 Contributions and Significance. We present a novel distributed displacement-based time-varying formation control approach for networks of heterogeneous planar underactuated vehicles without global position measurements. Specifically,

(1) Since vehicle networks are rarely homogeneous due to variety of sizes, capabilities, and mediums of operation, we do not assume any particular structure for the vehicle model thus allowing them to have non-identical dynamics. In other words, the formation control is designed for *heterogeneous* vehicle networks.
(2) Almost all vehicles in practice are underactuated, rendering the control laws with full actuation assumption impractical. This work applies to networks of *underactuated* vehicles. Since all fully actuated systems are feedback equivalent to the double-integrator dynamics, the formation control of heterogeneous fully actuated networks is equivalent to formation control of homogeneous double-integrator networks. Thus, we emphasize that the problem of formation control of *heterogeneous underactuated* networks is essentially different from and far more complicated than formation control of fully actuated networks.
(3) The proposed formation control law is distributed, i.e., it requires only neighbor-to-neighbor information exchange, and it does *not* require any *global position measurements*. We emphasize that the requirement of "without global position measurements" is an essential difficulty of distributed control. Moreover, the formation can be *time-varying*, which is useful in many applications, particularly when the shape of formation must change to avoid obstacles or collisions with other vehicles.

Compared with existing results in the literature and in contrast to existing controllers in Refs. [10], [20–25], and [27–32], which are applicable only to homogeneous vehicle networks, the approach proposed in this article can be applied to heterogeneous underactuated vehicle networks. In contrast to our previous coordination methods in Refs. [24] and [37], the approach proposed in this work can be used in time-varying formation. In contrast to the formation strategy in Ref. [34], the proposed approach does not require global position measurements of the followers, and guarantees uniform global asymptotic stability (UGAS) of the closed-loop system subject to bounded uncertainties and disturbances.

1.3 Outline. Section 2 presents the preliminaries and problem formulation. The feasible trajectory generation and the reduced order error dynamics are proposed in Sec. 3. In Sec. 4, a nonlinear control design for time-varying formation of a network of heterogeneous planar underactuated vehicles is presented. Section 5 applies the proposed control approach to various types of planar vehicles. Simulation results are shown in Sec. 6. Section 7 offers the concluding remarks.

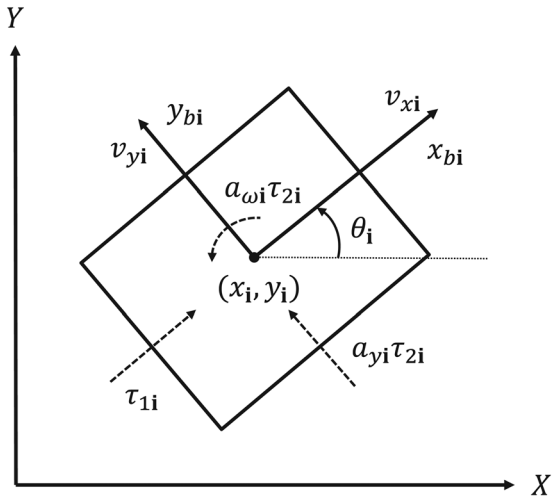

Fig. 1 Generic planar underactuated vehicle model of agent i

2 Preliminaries and Problem Formulation

2.1 Notations. The notations are standard in this paper. Let $\mathbb{R}^n$ represent the n-dimensional Euclidean space; $\mathbb{R}_{\geq 0}$ the set of all non-negative real numbers; $|\cdot|$ the Euclidean norm of vectors in $\mathbb{R}^n$; the diagonal matrix. Throughout this paper, we omit the arguments of functions when they are clear from the context. For multi-agent systems considered in this paper, we use the bold and nonitalicized subscript **i** to denote the index of an agent.

2.2 Planar Underactuated Vehicle Model. Without loss of generality, a planar underactuated vehicle can be modeled as a three degree-of-freedom planar rigid body with only two independent control inputs. The motion of a single vehicle **i** is described by assigning the body-fixed frame $\{x_{bi}, y_{bi}\}$ to its center of mass at $[x_i, y_i]^\top$ relative to a fixed frame $\{X, Y\}$ and orientation angle θ_i, as shown in Fig. 1. The general planar vehicle model is represented by the kinematic and force–balance equations of motion as

$$\begin{cases} \dot{x}_i = v_{xi}\cos\theta_i - v_{yi}\sin\theta_i \\ \dot{y}_i = v_{xi}\sin\theta_i + v_{yi}\cos\theta_i \\ \dot{\theta}_i = \omega_i \\ \dot{v}_{xi} = f_{xi}(v_{xi}, v_{yi}, \omega_i, \theta_i, t) + \delta_{xi}(t) + \tau_{1i} \\ \dot{v}_{yi} = f_{yi}(v_{xi}, v_{yi}, \omega_i, \theta_i, t) + \delta_{yi}(t) + a_{yi}\tau_{2i} \\ \dot{\omega}_i = f_{\omega i}(v_{xi}, v_{yi}, \omega_i, \theta_i, t) + \delta_{\omega i}(t) + a_{\omega i}\tau_{2i} \end{cases} \tag{1}$$

where $[v_{xi}, v_{yi}]^\top$ represents the body-fixed velocity, ω_i is the angular velocity, τ_{1i} and τ_{2i} are the control inputs. The constant coefficients a_{yi} and $a_{\omega i} \neq 0$ determine the contribution of τ_{2i} to sway and yaw motions, respectively. In addition, $f_{xi}(\cdot), f_{yi}(\cdot), f_{\omega i}(\cdot)$ are known locally Lipschitz continuous functions, and $\delta_{xi}(\cdot), \delta_{yi}(\cdot), \delta_{\omega i}(\cdot)$ stand for the unknown but bounded model uncertainties and disturbances, i.e.,

$$|\delta_{xi}(t)| \leq \Delta_{xi}, \quad |\delta_{yi}(t)| \leq \Delta_{yi}, \quad |\delta_{\omega i}(t)| \leq \Delta_{\omega i} \tag{2}$$

for all $t \geq 0$, where $\Delta_{x\mathbf{i}}, \Delta_{y\mathbf{i}}, \Delta_{\omega\mathbf{i}}$ are known positive constants. It is noted that although the force–balance equations may take various forms, such as Euler–Lagrange equations or port-controlled Hamiltonian form, we leave these equations undefined since our control design is generic and applicable to any of these forms.

From rigid body dynamics, the term $f_{y\mathbf{i}}(\cdot)$ in the sway force-balance equation in Eq. (1) consists of quadratic Coriolis and centrifugal force terms $f_{y\mathbf{i}}^{\mathrm{C}}(\cdot)$ and damping terms $f_{y\mathbf{i}}^{\mathrm{D}}(\cdot)$, i.e., $f_{y\mathbf{i}} = f_{y\mathbf{i}}^{\mathrm{C}} + f_{y\mathbf{i}}^{\mathrm{D}}$. The Coriolis force has the form $-m_{\mathbf{i}}\boldsymbol{\omega}_{\mathbf{i}} \times \mathbf{v}_{\mathbf{i}}$, and the centrifugal force has the form $-m_{\mathbf{i}}\boldsymbol{\omega}_{\mathbf{i}} \times (\boldsymbol{\omega}_{\mathbf{i}} \times \mathbf{r}_{\mathbf{i}})$, where $m_{\mathbf{i}}$ is the mass of the rigid body, $\boldsymbol{\omega}_{\mathbf{i}}$ is the angular velocity vector, $\mathbf{r}_{\mathbf{i}}$ and $\mathbf{v}_{\mathbf{i}}$ are the position and velocity vectors relative to the rotating reference frame, , respectively. Thus, the components of Coriolis and centrifugal forces in the sway direction are only functions of $v_{x\mathbf{i}}$ and $\omega_{\mathbf{i}}$, that is, $f_{y\mathbf{i}}^{\mathrm{C}} = f_{y\mathbf{i}}^{\mathrm{C}}(v_{x\mathbf{i}}, \omega_{\mathbf{i}})$, and the directions of the forces are opposite to the $y_{b\mathbf{i}}$ direction. Furthermore, the component of the damping force in the direction $y_{b\mathbf{i}}$ is only related to $v_{y\mathbf{i}}$, that is $f_{y\mathbf{i}}^{\mathrm{D}} = f_{y\mathbf{i}}^{\mathrm{D}}(v_{y\mathbf{i}})$, and its direction is opposite to the direction of $v_{y\mathbf{i}}$. Based on the above discussion, we make the following assumption on the underactuated force–balance equation of the vehicle dynamics considered in this paper.

ASSUMPTION 1. *There exists a constant $\eta_{\mathbf{i}} > 0$ related to the inertia parameters such that*

$$\frac{\partial f_{y\mathbf{i}}(v_{x\mathbf{i}}, v_{y\mathbf{i}}, \omega_{\mathbf{i}}, \theta_{\mathbf{i}}, t)}{\partial v_{x\mathbf{i}}} = -\eta_{\mathbf{i}}\omega_{\mathbf{i}} \tag{3}$$

and the direction of hydrodynamic damping force is opposite to the direction of $v_{y\mathbf{i}}$, that is,

$$\frac{\partial f_{y\mathbf{i}}(v_{x\mathbf{i}}, v_{y\mathbf{i}}, \omega_{\mathbf{i}}, \theta_{\mathbf{i}}, t)}{\partial v_{y\mathbf{i}}} \leq 0 \tag{4}$$

Remark 1. The conditions (3) and (4), which come from the rigid body assumption of the planar vehicle system, do not present real limitations since they are satisfied in planar vehicle models and robotic systems in general. The general form of Euler–Lagrangian equations for planar vehicle systems has an invertible generalized mass matrix. Condition (3) is satisfied since the centrifugal and Coriolis matrix is skew-symmetric, and condition (4) is satisfied since the damping matrix is positive semidefinite.

2.3 Graph Theory. Consider a network of $N+1$ heterogeneous planar underactuated vehicles, where the vehicles are numbered $\mathbf{i} = 0, 1, \ldots, N$ with $\mathbf{0}$ representing the group leader, which can be either a virtual vehicle or an actual vehicle, and $\mathbf{1}, \ldots, \mathbf{N}$ the followers. For formation control of planar underactuated vehicle networks, we use graphs to define the communication interaction among the vehicles [38]. The network topology is associated with a directed graph $\mathcal{G} = (\mathcal{V}, \mathcal{E})$ having $N+1$ nodes with node dynamics (1), where $\mathcal{V} = \{0, 1, \ldots, N\}$ and $\mathcal{E} \subseteq \mathcal{V} \times \mathcal{V}$ are the set of vertices and edges, respectively. We denote by $(\mathbf{i}, \mathbf{j}) \in \mathcal{E}$ the fact that node $\mathbf{j}$ can obtain information from node $\mathbf{i}$ for feedback control purposes. The set of neighboring nodes that communicate their information to node $\mathbf{i}$ is denoted by $\mathcal{N}_{\mathbf{i}} = \{\mathbf{j} \mid (\mathbf{j}, \mathbf{i}) \in \mathcal{E}\}$, i.e., the set of nodes with edges incoming to $\mathbf{i}$, as shown in Fig. 2. Let $w_{\mathbf{ij}}$ be a real number associated with the edge $(\mathbf{j}, \mathbf{i})$ for any $\mathbf{i}, \mathbf{j} \in \mathcal{V}$, representing the weighting coefficients of the communication between the vehicles. The physical meaning of the weighting coefficients $w_{\mathbf{ij}}$ represents the different levels of importance of the agent neighbors' information states. We assume that $w_{\mathbf{ij}} > 0$ if $(\mathbf{j}, \mathbf{i}) \in \mathcal{E}$ and $w_{\mathbf{ij}} = 0$, otherwise such that $\sum_{\mathbf{j} \in \mathcal{N}_{\mathbf{i}}} w_{\mathbf{ij}} = 1$. We make the following assumption on the communication topology graph considered in this paper.

ASSUMPTION 2. There exists at least one directed path starting from the group leader to any other agent in the network captured by the communication graph $\mathcal{G}$, which implies that the graph $\mathcal{G}$ contains a directed spanning tree. The group leader does not receive information from any other agent. Moreover, we assume that no self-loop or loop is allowed in the graph $\mathcal{G}$.

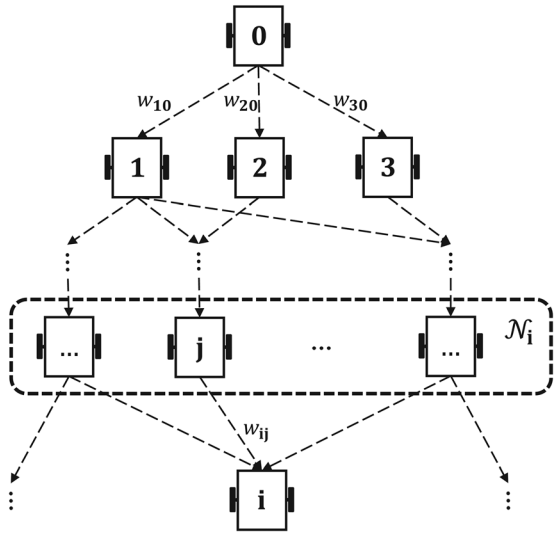

Fig. 2 Communication graph of $N+1$ heterogeneous vehicle network

2.4 Problem Formulation. The formation control problem is to design a distributed control protocol such that the network of heterogeneous planar vehicles moves together following the leader and asymptotically converge to as predefined geometric pattern, which can be either time-invariant or time-varying. The desired geometric pattern of the vehicle formation is defined by a set of time-varying offset vectors $d_{\mathbf{ij}}(t) \in \mathbb{R}^3$, $\mathbf{i}, \mathbf{j} = 0, 1, \ldots, N$, $\forall t \geq 0$. We denote the configuration variables of agent $\mathbf{i}$ as $q_{\mathbf{i}} = [x_{\mathbf{i}}, y_{\mathbf{i}}, \theta_{\mathbf{i}}]^{\top}$.

Formation control problem: Design distributed control laws for each follower agent without global position measurements such that: (i) the solutions of the closed-loop system are uniformly bounded; (ii) all the vehicles in the network can maintain a prescribed formation in the sense that

$$\lim_{t \to \infty} \left[q_{\mathbf{i}} - \sum_{\mathbf{j} \in \mathcal{N}_{\mathbf{i}}} w_{\mathbf{ij}} [q_{\mathbf{j}} + d_{\mathbf{ij}}(t)] \right] = 0, \ \forall \mathbf{i} \in \mathcal{V} \tag{5}$$

3 Feasible Trajectory and Error Dynamics

3.1 Feasible Trajectory Generation. Unlike fully actuated systems, underactuated system cannot be commanded to track arbitrary trajectories. Similarly, the desired configuration trajectory also cannot be assigned arbitrarily in formation. In other words, the time-varying offset $d_{\mathbf{ij}}(t) = [d_{\mathbf{ij}}^x(t), d_{\mathbf{ij}}^y(t), d_{\mathbf{ij}}^\theta(t)]^{\top}$ cannot be assigned to each vehicle arbitrarily. For a planar vehicle with one degree of underactuation, the time-varying offset vector can only be independently specified for two elements. The first two elements $d_{\mathbf{ij}}^x(t)$ and $d_{\mathbf{ij}}^y(t)$ are specified for the formation, which assign the desired position trajectory of the follower agent $\mathbf{i}$ relative to that of its neighbor $\mathbf{j} \in \mathcal{N}_{\mathbf{i}}$. Then, the orientation offset $d_{\mathbf{ij}}^\theta(t)$ must be determined from the vehicle dynamics. Specifically, let us denote the desired position trajectory assigned to agent $\mathbf{i}$ from all agents $\mathbf{j} \in \mathcal{N}_{\mathbf{i}}$ by

$$\bar{x}_{\mathbf{i}}(t) := \sum_{\mathbf{j} \in \mathcal{N}_{\mathbf{i}}} w_{\mathbf{ij}} [x_{\mathbf{j}} + d_{\mathbf{ij}}^x(t)], \quad \bar{y}_{\mathbf{i}}(t) := \sum_{\mathbf{j} \in \mathcal{N}_{\mathbf{i}}} w_{\mathbf{ij}} [y_{\mathbf{j}} + d_{\mathbf{ij}}^y(t)] \tag{6}$$

Then, the feasible orientation trajectory $\bar{\theta}_{\mathbf{i}}(t)$ needs to be determined based on the nonholonomic constraint of agent $\mathbf{i}$. It follows

from Eq. (1) that the desired orientation trajectory $\bar{\theta}_{\mathbf{i}}(t)$ is a solution of the following second-order ordinary differential equation:

$$\dot{\bar{v}}_{y\mathbf{i}}(t) = f_{y\mathbf{i}}\big(\bar{v}_{x\mathbf{i}}(t), \bar{v}_{y\mathbf{i}}(t), \bar{\omega}_{\mathbf{i}}(t), \bar{\theta}_{\mathbf{i}}(t), t\big) + \frac{a_{y\mathbf{i}}}{a_{\omega\mathbf{i}}}\left[\dot{\bar{\omega}}_{\mathbf{i}}(t) - f_{\omega\mathbf{i}}\big(\bar{v}_{x\mathbf{i}}(t), \bar{v}_{y\mathbf{i}}(t), \bar{\omega}_{\mathbf{i}}(t), \bar{\theta}_{\mathbf{i}}(t), t\big)\right] \tag{7}$$

Subject to initial conditions $\bar{\theta}_{\mathbf{i}}(0) = \bar{\theta}_{\mathbf{i},0}$ and $\dot{\bar{\theta}}_{\mathbf{i}}(0) = \dot{\bar{\theta}}_{\mathbf{i},0}$, and $\bar{v}_{x\mathbf{i}}(t)$, $\bar{v}_{y\mathbf{i}}(t)$, and $\bar{\omega}_{\mathbf{i}}(t)$ are given by

$$\begin{bmatrix} \bar{v}_{x\mathbf{i}}(t) \\ \bar{v}_{y\mathbf{i}}(t) \\ \bar{\omega}_{\mathbf{i}}(t) \end{bmatrix} = \begin{bmatrix} \cos\bar{\theta}_{\mathbf{i}}(t) & \sin\bar{\theta}_{\mathbf{i}}(t) & 0 \\ -\sin\bar{\theta}_{\mathbf{i}}(t) & \cos\bar{\theta}_{\mathbf{i}}(t) & 0 \\ 0 & 0 & 1 \end{bmatrix} \begin{bmatrix} \dot{\bar{x}}_{\mathbf{i}}(t) \\ \dot{\bar{y}}_{\mathbf{i}}(t) \\ \dot{\bar{\theta}}_{\mathbf{i}}(t) \end{bmatrix}$$

It is noted that no global position measurement is required in Eq. (7). Next, the feasible orientation trajectory $\bar{\theta}_{\mathbf{i}}(t)$ can be calculated by numerically integrating Eq. (7) given any smooth position offset $[d^x_{\mathbf{ij}}(t), d^y_{\mathbf{ij}}(t)]^\top$. Furthermore, the feasible orientation offset variable $d^\theta_{\mathbf{ij}}(t)$ is selected as $d^\theta_{\mathbf{ij}}(t) = \bar{\theta}_{\mathbf{i}}(t) - \theta_{\mathbf{j}}(t)$.

Remark 2. The second-order ordinary differential Eq. (7) reduces into a first order ordinary differential equation in the case of $a_{y\mathbf{i}} = 0$. We emphasize that only the local motion information (velocity and acceleration) are used in feasible trajectory generation. The formation is achieved if $x_{\mathbf{i}} \to \bar{x}_{\mathbf{i}}(t)$, $y_{\mathbf{i}} \to \bar{y}_{\mathbf{i}}(t)$, and $\theta_{\mathbf{i}} \to \bar{\theta}_{\mathbf{i}}(t)$. In the control design, we will use the differences $(x_{\mathbf{i}} - \bar{x}_{\mathbf{i}}(t))$ and $(y_{\mathbf{i}} - \bar{y}_{\mathbf{i}}(t))$ for feedback purpose, and only relative position measurements $(x_{\mathbf{i}} - x_{\mathbf{j}})$ and $(y_{\mathbf{i}} - y_{\mathbf{j}})$ are required to construct these difference signals.

3.2 Reduced Order Error Dynamics. In this section, we introduce a transformation that results in reduced order error dynamics. Define the new formation errors $z_{\mathbf{i}} = [z_{1\mathbf{i}}, z_{2\mathbf{i}}, z_{3\mathbf{i}}]^\top$ for agents $\mathbf{i} = 1, \ldots, N$ as

$$z_{\mathbf{i}} = J(\theta_{\mathbf{i}})^\top[(\dot{q}_{\mathbf{i}} - \dot{\bar{q}}_{\mathbf{i}}) - \Lambda(q_{\mathbf{i}} - \bar{q}_{\mathbf{i}})] \tag{8}$$

where $\bar{q}_{\mathbf{i}} := [\bar{x}_{\mathbf{i}}, \bar{y}_{\mathbf{i}}, \bar{\theta}_{\mathbf{i}}]^\top$, the matrix

$$J(\theta_{\mathbf{i}}) := \begin{bmatrix} \cos\theta_{\mathbf{i}} & -\sin\theta_{\mathbf{i}} & 0 \\ \sin\theta_{\mathbf{i}} & \cos\theta_{\mathbf{i}} & 0 \\ 0 & 0 & 1 \end{bmatrix} \tag{9}$$

and $\Lambda := \mathrm{diag}\{\lambda_1, \lambda_2, \lambda_3\}$ with λ_1, λ_2, $\lambda_3 < 0$. The idea is that when the error vector $z_{\mathbf{i}}(t)$ asymptotically converges to 0, all configuration errors asymptotically converge to 0 as $t \to \infty$, as stated in the following lemma.

LEMMA 1. *Consider the error $z_{\mathbf{i}}$ defined in Eq. (8), where $\Lambda := \mathrm{diag}\{\lambda_1, \lambda_2, \lambda_3\}$ with λ_1, λ_2, $\lambda_3 < 0$. If the error $|z_{\mathbf{i}}(t)| \to 0$ as $t \to \infty$, then the formation error $|q_{\mathbf{i}}(t) - \bar{q}_{\mathbf{i}}(t)| \to 0$ as $t \to \infty$.*

Proof. Since $J(\theta_{\mathbf{i}})^\top$ is an orthogonal matrix, $|z_{\mathbf{i}}(t)| \to 0$ implies $|(\dot{q}_{\mathbf{i}} - \dot{\bar{q}}_{\mathbf{i}}) - \Lambda(q_{\mathbf{i}} - \bar{q}_{\mathbf{i}})| \to 0$, which also can be written as a perturbed linear system

$$\dot{\tilde{q}}_{\mathbf{i}} = \Lambda\tilde{q}_{\mathbf{i}} + \zeta_{\mathbf{i}}(t), \quad \lim_{t\to\infty} |\zeta_{\mathbf{i}}(t)| = 0 \tag{10}$$

where $\tilde{q}_{\mathbf{i}} := q_{\mathbf{i}} - \bar{q}_{\mathbf{i}}(t)$, and $\zeta_{\mathbf{i}}(t) = J(\theta_{\mathbf{i}})z_{\mathbf{i}}(t)$. The nominal part $\dot{\tilde{q}}_{\mathbf{i}} = \Lambda\tilde{q}_{\mathbf{i}}$ of the perturbed linear system is exponentially stable, and the perturbation term $\zeta_{\mathbf{i}}(t)$ converges to zero as $t \to \infty$. Then, by the converging-input-converging-state property of stable linear systems [39], we conclude that $|\tilde{q}_{\mathbf{i}}(t)| \to 0$, and $|\dot{\tilde{q}}_{\mathbf{i}}(t)| \to 0$ as $t \to \infty$. ■

Thus, the control objective is then to design a controller, which asymptotically stabilize the formation errors $z_{\mathbf{i}}(t)$ for all agents $\mathbf{i} = 1, \ldots, N$. The reduced order error dynamics for agent $\mathbf{i}$ are calculated by taking derivative of Eq. (8) along the trajectory of Eq. (1) as

$$\dot{z}_{\mathbf{i}} = \dot{J}(\theta_{\mathbf{i}})^\top(\dot{\tilde{q}}_{\mathbf{i}} - \Lambda\tilde{q}_{\mathbf{i}}) + J(\theta_{\mathbf{i}})^\top(\ddot{\tilde{q}}_{\mathbf{i}} - \Lambda\dot{\tilde{q}}_{\mathbf{i}}) \tag{11}$$

Substituting Eq. (1) for agents $\mathbf{i}$ and $\mathbf{j}$ into the error dynamics (11), and using the following feedback transformation:

$$\begin{aligned} \tau_{1\mathbf{i}} = &-f_{x\mathbf{i}} + \omega_{\mathbf{i}}v_{y\mathbf{i}} + \cos(\theta_{\mathbf{i}} - \bar{\theta}_{\mathbf{i}})(\dot{\bar{v}}_{x\mathbf{i}} - \bar{\omega}_{\mathbf{i}}\bar{v}_{y\mathbf{i}}) \\ &+ \sin(\theta_{\mathbf{i}} - \bar{\theta}_{\mathbf{i}})(\dot{\bar{v}}_{y\mathbf{i}} + \bar{\omega}_{\mathbf{i}}\bar{v}_{x\mathbf{i}}) + \lambda_1 v_{x\mathbf{i}} \\ &-\lambda_1[\bar{v}_{x\mathbf{i}}\cos(\theta_{\mathbf{i}} - \bar{\theta}_{\mathbf{i}}) + \bar{v}_{y\mathbf{i}}\sin(\theta_{\mathbf{i}} - \bar{\theta}_{\mathbf{i}})] + u_{1\mathbf{i}} \end{aligned} \tag{12}$$

$$\tau_{2\mathbf{i}} = \frac{1}{a_{\omega\mathbf{i}}}\left[-f_{\omega\mathbf{i}} + \dot{\bar{\omega}}_{\mathbf{i}} + \lambda_3(\omega_{\mathbf{i}} - \bar{\omega}_{\mathbf{i}}) + u_{2\mathbf{i}}\right] \tag{13}$$

the reduced order error dynamics (11) can be written as

$$\begin{bmatrix} \dot{z}_{1\mathbf{i}} \\ \dot{z}_{2\mathbf{i}} \\ \dot{z}_{3\mathbf{i}} \end{bmatrix} = \begin{bmatrix} \omega_{\mathbf{i}}z_{2\mathbf{i}} \\ -\omega_{\mathbf{i}}z_{1\mathbf{i}} \\ 0 \end{bmatrix} + \begin{bmatrix} u_{1\mathbf{i}} \\ \Psi_{\mathbf{i}} \\ u_{2\mathbf{i}} \end{bmatrix} + \begin{bmatrix} \delta_{x\mathbf{i}}(t) \\ \delta_{y\mathbf{i}}(t) \\ \delta_{\omega\mathbf{i}}(t) \end{bmatrix} \tag{14}$$

where

$$\begin{aligned} \Psi_{\mathbf{i}} = &\dot{v}_{y\mathbf{i}} + \omega_{\mathbf{i}}v_{x\mathbf{i}} + \sin(\theta_{\mathbf{i}} - \bar{\theta}_{\mathbf{i}})(\dot{\bar{v}}_{x\mathbf{i}} - \bar{\omega}_{\mathbf{i}}\bar{v}_{y\mathbf{i}}) \\ &-\cos(\theta_{\mathbf{i}} - \bar{\theta}_{\mathbf{i}})(\dot{\bar{v}}_{y\mathbf{i}} + \bar{\omega}_{\mathbf{i}}\bar{v}_{x\mathbf{i}}) - \lambda_2 v_{y\mathbf{i}} \\ &+\lambda_2[-\bar{v}_{x\mathbf{i}}\sin(\theta_{\mathbf{i}} - \bar{\theta}_{\mathbf{i}}) + \bar{v}_{y\mathbf{i}}\cos(\theta_{\mathbf{i}} - \bar{\theta}_{\mathbf{i}})] \end{aligned} \tag{15}$$

The error dynamics (14) has only three states for each agent that must be stabilized to achieve the desired formation. Next, we will design the new control inputs $[u_{1\mathbf{i}}, u_{2\mathbf{i}}]^\top$ to stabilize the reduced order error dynamics (14) for all agents $\mathbf{i} = 1, \ldots, N$. The control law will be distributed and will not use global position measurements since (14) only depends on relative pose of agent $\mathbf{i}$ with respect to its neighbor $\mathbf{j}$ and their velocities and accelerations in their own body-fixed frames measured by onboard sensors such as Lidar, camera, inertial measurement unit, and speedometer.

3.3 Technical Lemmas. In this section, we review and develop some results needed for the main results of the paper.

LEMMA 2 ([40, restated]). *Consider the following system:*

$$\begin{aligned} \dot{x}_1 &= f(t, x_1) + \omega(t)x_2 \\ \dot{x}_2 &= -p\,\omega(t)^\top\left[\frac{\partial V}{\partial x_1}\right]^\top \end{aligned} \tag{16}$$

where $x_1 \in \mathbb{R}^{n_1}, x_2 \in \mathbb{R}, f : \mathbb{R}_{\geq 0} \times \mathbb{R}^{n_1} \to \mathbb{R}^{n_1}, \omega : \mathbb{R}_{\geq 0} \to \mathbb{R}^{n_1}, V : \mathbb{R}_{\geq 0} \times \mathbb{R}^{n_1} \to \mathbb{R}_{\geq 0}$ and $p > 0$ is a constant. Let the following Assumptions A1–A3 hold.

ASSUMPTION 1. *There exist class $\mathcal{K}_\infty$ functions $\alpha_1(\cdot)$ and $\alpha_2(\cdot)$, and a positive definite function $\alpha_3(\cdot)$ such that, for all $t \geq 0$, and $x_1 \in \mathbb{R}^{n_1}$*

$$\begin{aligned} \alpha_1(|x_1|) \leq V(t, x_1) \leq \alpha_2(|x_2|), \\ \frac{\partial V}{\partial t} + \frac{\partial V}{\partial x_1}f(t, x_1) \leq -\alpha_3(|x_1|), \text{ a.e.} \end{aligned}$$

ASSUMPTION 2. *There exists a continuous nondecreasing function $\beta : \mathbb{R}_{\geq 0} \to \mathbb{R}_{\geq 0}$ such that, for all $t \geq 0$, and $x_1 \in \mathbb{R}^{n_1}$*

$$\max\left\{|f(t, x_1)|, \left|\frac{\partial V(t, x_1)}{\partial x_1}\right|\right\} \leq \beta(|x_1|)|x_1|, \text{ a.e.}$$

ASSUMPTION 3. *The function $\omega(\cdot)$ is bounded with a bounded first derivative, smooth and persistently exciting (PE), i.e., there exist $T > 0, \mu > 0$ such that*

$$\int_t^{t+T} |\omega(\tau)|^2 \mathrm{d}\tau \geq \mu, \ \forall t \geq 0$$

Then the origin of Eq. (16) is UGAS. Furthermore, if the origin of system $\dot{x}_1 = f(t, x_1)$ is uniformly globally exponentially stable (UGES), then the origin of Eq. (16) is UGES.

The next lemma presents a cascaded-like property of the error dynamics (14), which suggests to separately control the linear and angular dynamics, and is important in the control design.

LEMMA 3. *Let Assumption 1 hold. Under feedback transformation (12), (13), if both $z_{3\mathbf{i}}(t)$ and $|[u_{1\mathbf{i}}(t), u_{2\mathbf{i}}(t)]|$ converge to zero exponentially as $t \to \infty$, and $\bar{\omega}_{\mathbf{i}}(t)$ is bounded and PE, then the interconnected term $\Psi_{\mathbf{i}}(t) \to 0$ exponentially as $t \to \infty$.*

Proof. It follows from Lemma 1 that $z_{3\mathbf{i}}(t) \to 0$ exponentially implies $(\theta_{\mathbf{i}}(t) - \bar{\theta}_{\mathbf{i}}(t)) \to 0$ and $(\dot{\theta}_{\mathbf{i}}(t) - \dot{\bar{\theta}}_{\mathbf{i}}(t)) \to 0$ exponentially as $t \to \infty$. Consequently, $\sin(\theta_{\mathbf{i}}(t) - \bar{\theta}_{\mathbf{i}}(t)) \to 0$ and $\cos(\theta_{\mathbf{i}}(t) - \bar{\theta}_{\mathbf{i}}(t)) \to 1$ exponentially. Then, from Eq. (12), we have

$$(\dot{v}_{x\mathbf{i}} - \dot{\bar{v}}_{x\mathbf{i}}) = \lambda_1 (v_{x\mathbf{i}} - \bar{v}_{x\mathbf{i}}) + \bar{\omega}_{\mathbf{i}} (v_{y\mathbf{i}} - \bar{v}_{y\mathbf{i}}) + o_x(t) \tag{17}$$

where $o_x(t) \to 0$ exponentially, and from the model (1), we have

$$\begin{aligned}(\dot{v}_{y\mathbf{i}} - \dot{\bar{v}}_{y\mathbf{i}}) = {} & f_{y\mathbf{i}}(v_{x\mathbf{i}}, v_{y\mathbf{i}}, \omega_{\mathbf{i}}, \theta_{\mathbf{i}}, t) + a_{y\mathbf{i}} \tau_{2\mathbf{i}} \\ & - f_{y\mathbf{i}}(\bar{v}_{x\mathbf{i}}, \bar{v}_{y\mathbf{i}}, \bar{\omega}_{\mathbf{i}}, \bar{\theta}_{\mathbf{i}}, t) - a_{y\mathbf{i}} \bar{\tau}_{2\mathbf{i}}\end{aligned} \tag{18}$$

Then, the feedback transformation (13) implies that $(\tau_{2\mathbf{i}} - \bar{\tau}_{2\mathbf{i}}) \to 0$, and using the conditions (3) and (4) in Assumption 1, (17) and (18) can be written as

$$\begin{bmatrix} \dot{v}_{x\mathbf{i}} - \dot{\bar{v}}_{x\mathbf{i}} \\ \dot{v}_{y\mathbf{i}} - \dot{\bar{v}}_{y\mathbf{i}} \end{bmatrix} = \begin{bmatrix} \lambda_1 & \bar{\omega}_{\mathbf{i}}(t) \\ -\eta_{\mathbf{i}} \bar{\omega}_{\mathbf{i}}(t) & \mathcal{A}_{22}(t) \end{bmatrix} \begin{bmatrix} v_{x\mathbf{i}} - \bar{v}_{x\mathbf{i}} \\ v_{y\mathbf{i}} - \bar{v}_{y\mathbf{i}} \end{bmatrix} + o(t) \tag{19}$$

where $\mathcal{A}_{22}(t) = \partial f_{y\mathbf{i}} / \partial v_{y\mathbf{i}} \leq 0$ and $|o(t)| \to 0$ exponentially. Note that the system (19) can be seen as a linear time-varying system under a exponentially converging input $o(t)$, and the nominal part of Eq. (19) with $\mathcal{A}_{22}(t) \equiv 0$ is reminiscent of the system (16) in Lemma 2. Since $\lambda_1 < 0$ and $\mathcal{A}_{22}(t) \leq 0$, referring to Lemma 2, the comparison lemma, and converging-input-converging-state property of linear systems, we conclude that system (19) is UGES provided that $\bar{\omega}_{\mathbf{i}}(t)$ is bounded and PE. On the other hand, it follows from Eq. (15) that:

$$\Psi_{\mathbf{i}} \to (\dot{v}_{y\mathbf{i}} - \dot{\bar{v}}_{y\mathbf{i}}) - \lambda_2 (v_{y\mathbf{i}} - \bar{v}_{y\mathbf{i}}) + \bar{\omega}_{\mathbf{i}}(t)(v_{x\mathbf{i}} - \bar{v}_{x\mathbf{i}}) \tag{20}$$

and from the UGES of Eq. (19), we conclude that $\Psi_{\mathbf{i}}(t) \to 0$ exponentially as $t \to \infty$. ■

4 Nonlinear Control Design

We begin this section by noting that different control laws may be applied to stabilize the error dynamics (14), for instance, sliding mode control, backstepping design, or linear high-gain feedback. While *any* nonlinear control technique may be applicable under this framework, in this paper, we choose sliding mode control due its simplicity and robustness, which only requires boundedness of unknown modeling uncertainties and disturbances.

First, it is noted that the error dynamics (14) is structured such that the angular error $z_{3\mathbf{i}}$ is decoupled from the positioning error $[z_{1\mathbf{i}}, z_{2\mathbf{i}}]^\top$, and thus can be independently controlled. Therefore, we choose the simplest sliding mode control law as

$$u_{2\mathbf{i}} = -k_{2\mathbf{i}} \operatorname{sign}(z_{3\mathbf{i}}) \tag{21}$$

where $k_{2\mathbf{i}} > \Delta_{\omega\mathbf{i}}$ implying that $z_{3\mathbf{i}}$ is stabilized to zero in finite time. It follows from Lemma 1 that angular error will converge to zero as $t \to \infty$. Next, consider the linear error dynamics $(z_{1\mathbf{i}}, z_{2\mathbf{i}})$. We define the sliding variable in the following form:

$$s_{\mathbf{i}}(z_{1\mathbf{i}}, z_{2\mathbf{i}}, t) = -\omega_{\mathbf{i}} z_{1\mathbf{i}} + \Psi_{\mathbf{i}}(t) + c_{\mathbf{i}} z_{2\mathbf{i}} \tag{22}$$

where $c_{\mathbf{i}} > 0$ is a constant. Referring to (14), the dynamics on the sliding manifold $\{s_{\mathbf{i}} = 0\}$ are given by

$$\dot{z}_{2\mathbf{i}} = -c_{\mathbf{i}} z_{2\mathbf{i}} + \delta_{y\mathbf{i}}(t) \tag{23}$$

where the nominal part is an exponential stable linear system. If the mismatched uncertainty $\delta_{y\mathbf{i}}(\cdot)$ has a linear growth bound with respect to $z_{2\mathbf{i}}$, then the dynamics on the sliding manifold is globally exponential stable.

To derive the control law, let us consider the Lyapunov candidate $V_{\mathbf{i}}(s_{\mathbf{i}}) = \frac{1}{2} s_{\mathbf{i}}^2$ and take its time derivative along $(z_{1\mathbf{i}}, z_{2\mathbf{i}})$-trajectories as

$$\begin{aligned}\dot{V}_{\mathbf{i}}(t, z_{1\mathbf{i}}, z_{2\mathbf{i}}) = {} & s_{\mathbf{i}} \left[\frac{\partial s_{\mathbf{i}}}{\partial z_{1\mathbf{i}}} (\omega_{\mathbf{i}} z_{2\mathbf{i}} + u_{1\mathbf{i}} + \delta_{x\mathbf{i}}(t)) \right. \\ & \left. + \frac{\partial s_{\mathbf{i}}}{\partial t} + \frac{\partial s_{\mathbf{i}}}{\partial z_{2\mathbf{i}}} \left(-\omega_{\mathbf{i}} z_{1\mathbf{i}} + \Psi_{\mathbf{i}}(t) + \delta_{y\mathbf{i}}(t) \right) \right]\end{aligned} \tag{24}$$

Following standard sliding mode control approach and assuming $\partial s_{\mathbf{i}} / \partial z_{1\mathbf{i}} \neq 0$, we choose the control law as:

$$u_{1\mathbf{i}} = -\omega_{\mathbf{i}} z_{2\mathbf{i}} - \left(\frac{\partial s_{\mathbf{i}}}{\partial z_{1\mathbf{i}}} \right)^{-1} \left[\frac{\partial s_{\mathbf{i}}}{\partial z_{2\mathbf{i}}} (-\omega_{\mathbf{i}} z_{1\mathbf{i}} + \Psi_{\mathbf{i}}) + \frac{\partial s_{\mathbf{i}}}{\partial t} + k_{1\mathbf{i}} \operatorname{sign}(s_{\mathbf{i}}) \right] \tag{25}$$

which guarantees

$$\dot{V}_{\mathbf{i}}(t, z_{1\mathbf{i}}, z_{2\mathbf{i}}) \leq |s_{\mathbf{i}}| \left[-k_{1\mathbf{i}} + \left| \frac{\partial s_{\mathbf{i}}}{\partial z_{1\mathbf{i}}} \right| \Delta_{x\mathbf{i}} + \left| \frac{\partial s_{\mathbf{i}}}{\partial z_{2\mathbf{i}}} \right| \Delta_{y\mathbf{i}} \right] \tag{26}$$

The robustness gain $k_{1\mathbf{i}}$ is chosen such that

$$k_{1\mathbf{i}} > \left| \frac{\partial s_{\mathbf{i}}}{\partial z_{1\mathbf{i}}} \right| \Delta_{x\mathbf{i}} + \left| \frac{\partial s_{\mathbf{i}}}{\partial z_{2\mathbf{i}}} \right| \Delta_{y\mathbf{i}} \tag{27}$$

Then, trajectories will converge to the sliding manifold $\{s_{\mathbf{i}} = 0\}$ in finite time. On the sliding manifold, the dynamics are represented by Eq. (23) and exponential stability can be established under the linear growth bound assumption that $|\delta_{y\mathbf{i}}(\cdot)| \leq \kappa_{\mathbf{i}} |z_{2\mathbf{i}}|$, where $\kappa_{\mathbf{i}}$ is a positive constant [41, Lemma 9.1]. Note that $|\partial s_{\mathbf{i}} / \partial z_{1\mathbf{i}}| = |\omega_{\mathbf{i}}(t)|$ and $|\partial s_{\mathbf{i}} / \partial z_{2\mathbf{i}}| = c_{\mathbf{i}}$. For each vehicle $\mathbf{i}$, the maximum angular velocity must be bounded in practice, i.e., $|\omega_{\mathbf{i}}(t)| \leq \omega_{M\mathbf{i}}$ for all $t \geq 0$, and can be measured by experiments in advance. Thus, the robustness gain $k_{1\mathbf{i}}$ can be simply chosen such that $k_{1\mathbf{i}} > \omega_{M\mathbf{i}} \Delta_{x\mathbf{i}} + c_{\mathbf{i}} \Delta_{y\mathbf{i}}$ in practice. The following theorem presents the main results.

THEOREM 1. *Consider a network of heterogeneous planar underactuated vehicles, where the node dynamics given by Eq. (1) satisfy Assumption 1, with the communication topology satisfying Assumption 2. Assume that the linear and angular velocities and accelerations of the leader are bounded, the angular velocity for each follower $\mathbf{i}$ is nonzero, i.e., $\omega_{\mathbf{i}}(t) \neq 0$ for all $t \geq 0$, and the mismatched uncertainty $\delta_{y\mathbf{i}}(\cdot)$ has a linear growth bound, i.e., $|\delta_{y\mathbf{i}}(t)| \leq \kappa_{\mathbf{i}} |z_{2\mathbf{i}}|$ with $\kappa_{\mathbf{i}} > 0$. Then, under the control law (12), (13), (21), and (25) with control gains $c_{\mathbf{i}} > 0$, $k_{2\mathbf{i}} > \Delta_{\omega\mathbf{i}}$, and $k_{1\mathbf{i}}$ satisfying (27), the origin of error dynamics (14) is UGAS.*

Proof. Consider the Lyapunov function candidate for the error dynamics (14) as $W_{\mathbf{i}} = V_{\mathbf{i}}(s_{\mathbf{i}}) + \frac{1}{2} z_{3\mathbf{i}}^2$. From Eqs. (21) and (26), it follows that, along the trajectories of Eq. (14):

$$\begin{aligned}\dot{W}_{\mathbf{i}} \leq {} & - \left(k_{1\mathbf{i}} - \left| \frac{\partial s_{\mathbf{i}}}{\partial z_{1\mathbf{i}}} \right| \Delta_{x\mathbf{i}} - \left| \frac{\partial s_{\mathbf{i}}}{\partial z_{2\mathbf{i}}} \right| \Delta_{y\mathbf{i}} \right) |s_{\mathbf{i}}| - (k_{2\mathbf{i}} - \Delta_{\omega\mathbf{i}}) |z_{3\mathbf{i}}| \\ \leq {} & 0\end{aligned} \tag{28}$$

which implies that the closed-loop system is globally stable, and thus the formation error $z_{\mathbf{i}}$ is bounded over the time interval $[0, +\infty)$. Again, the variables $z_{3\mathbf{i}}(t)$ and $s_{\mathbf{i}}(t)$ converge to zero in finite time. It is noted that $z_{3\mathbf{i}} \to 0$ for all $\mathbf{i} = 1, \ldots, N$ implies that the error in angular motion for each agent will converge to zero as $t \to \infty$. Next, $s_{\mathbf{i}}(t)$ converges to zero in finite time implies that all trajectories will reach the sliding manifold, and on the manifold, $z_{2\mathbf{i}}(t) \to 0$ exponentially under the linear growth bound condition $|\delta_{y\mathbf{i}}(t)| \leq \kappa_{\mathbf{i}}|z_{2\mathbf{i}}|$, [41, Lemma 9.1]. Also, on the sliding manifold, we have $z_{1\mathbf{i}} \to \Psi_{\mathbf{i}}/\omega_{\mathbf{i}}$, and with the assumption $\partial s_{\mathbf{i}}/\partial z_{1\mathbf{i}} \neq 0$, we only need to verify that $\Psi_{\mathbf{i}}(t) \to 0$ as $t \to \infty$. It also follows from Eq. (22) that $\partial s_{\mathbf{i}}/\partial z_{1\mathbf{i}} \neq 0$ is equivalent to $\omega_{\mathbf{i}}(t) \neq 0$. Since $z_{3\mathbf{i}}(t) \to 0$ in finite time for all $\mathbf{i} = 1, \ldots, N$, then $(\theta_{\mathbf{i}} - \bar{\theta}_{\mathbf{i}}) \to 0$ and $(\dot{\theta}_{\mathbf{i}} - \dot{\bar{\theta}}_{\mathbf{i}}) \to 0$ as $t \to \infty$ with an exponential convergence rate λ_3. This implies that the orientations of all vehicles in the network are aligned with the predefined offset $d_{\mathbf{ij}}^{\theta}(t)$. Then, the control law (21) suggests that $u_{2\mathbf{i}}(t)$ reaches zero in finite time, and similarly, on the sliding manifold $\{s_{\mathbf{i}} = 0\}$ we have $u_{2\mathbf{i}}(t) \to 0$ exponentially as $t \to \infty$. It follows from Lemma 3 that $\Psi_{\mathbf{i}}(t) \to 0$ exponentially as $t \to \infty$, and consequently $z_{1\mathbf{i}}(t) \to 0$ as $t \to \infty$. Therefore, the UGES of the closed-loop error dynamics has been established. Finally, we conclude that the time-varying formation of heterogeneous planar underactuated vehicle network is achieved by Lemma 1. ■

Remark 3. As mentioned above, the singularity condition $\partial s_{\mathbf{i}}/\partial z_{1\mathbf{i}}(t) \neq 0$ implies that $\omega_{\mathbf{i}}(t) \neq 0$. In case of $\omega_{\mathbf{i}}(t) = 0$, the $(z_{1\mathbf{i}}, z_{2\mathbf{i}})$-dynamics are uncoupled, that is, $z_{2\mathbf{i}}$ cannot be controlled by the control input $u_{1\mathbf{i}}$. In this situation, a hybrid control law can be used to avoid singularity. Selecting $s_{\mathbf{i}} = z_{1\mathbf{i}}$, the control law (25) is replaced with $u_{1\mathbf{i}} = -k_{1\mathbf{i}}\,\mathrm{sign}(s_{\mathbf{i}})$, where $k_{1\mathbf{i}} > \Delta_{x\mathbf{i}}$. Then, the origin of the $(z_{1\mathbf{i}}, z_{3\mathbf{i}})$-subsystem is UGAS. Furthermore, disturbance observers (DOB) are widely used in the literature to estimate disturbances [42,43]. An efficient solution for counteracting the mismatched disturbances is known as disturbance observer-based sliding mode control (DOB-SMC) [44]. Thus, if the mismatched uncertainty $\delta_{y\mathbf{i}}(t)$ is nonvanishing, an DOB-SMC may be employed. In this case, the sliding variable (22) can be designed as $s_{\mathbf{i}}(z_{1\mathbf{i}}, z_{2\mathbf{i}}, t) = -\omega_{\mathbf{i}} z_{1\mathbf{i}} + \Psi_{\mathbf{i}}(t) + c_{\mathbf{i}} z_{2\mathbf{i}} + \hat{\delta}_{y\mathbf{i}}(t)$, where $\hat{\delta}_{y\mathbf{i}}(t)$ is the estimation of the $\delta_{y\mathbf{i}}(t)$. Then, the error dynamics (23) become $\dot{z}_{2\mathbf{i}} = -c_{\mathbf{i}} z_{2\mathbf{i}} + [\delta_{y\mathbf{i}}(t) - \hat{\delta}_{y\mathbf{i}}(t)]$, and correspondingly, the origin of the closed-loop system is UGAS if $\delta_{y\mathbf{i}}(t) - \hat{\delta}_{y\mathbf{i}}(t) \to 0$ as $t \to \infty$.

Remark 4. It is noted that $\dot{\bar{v}}_{x\mathbf{i}}(t)$, $\dot{\bar{v}}_{y\mathbf{i}}(t)$, and $\dot{\bar{\omega}}_{\mathbf{i}}(t)$ are required in the control law (12) and (13), which means that the acceleration information of each vehicle should be known. In some practical applications, the acceleration can be measured directly by onboard sensors. In other cases, the acceleration can be estimated in real-time using observers or differentiators. Various differentiators can be used to estimate the accelerations, for instance, the sliding mode differentiator [45], or the high-gain differentiator [46], etc. Furthermore, the estimation errors can be viewed as a part of the disturbances $\delta_{x\mathbf{i}}(t), \delta_{y\mathbf{i}}(t), \delta_{\omega\mathbf{i}}(t)$, which can be handled by the proposed controller.

5 Applications

The time-varying formation of heterogeneous vehicles can be applied in practical scenarios such as reconnaissance, surveillance, payload transport, cooperative search, and for military operations to increase the striking force from multiple sources on the ground, in the sea, and in the air, to name a few examples. Here, we present the specific forms of the generic terms in Eq. (1) for various vehicles including wheeled mobile robots, marine surface vessels, and PVTOL aircraft, and verify that conditions (3) and (4) in Theorem 1 are satisfied. The vehicle models are presented in the Appendix.

5.1 Mobile Robots. Consider the model of a differentially driven wheeled mobile robot **i** moving on a horizontal plane. The general terms introduced in Eq. (1) can be determined as [24]

$$f_{x\mathbf{i}} = \frac{m_{\mathbf{i}} d_{\mathbf{i}}}{\tilde{m}_{\mathbf{i}}}\omega_{\mathbf{i}}^2,\ f_{y\mathbf{i}} = -\frac{m_{\mathbf{i}} d_{\mathbf{i}}^2}{\tilde{I}_{\mathbf{i}}}\omega_{\mathbf{i}} v_{x\mathbf{i}},\quad f_{\omega\mathbf{i}} = -\frac{m_{\mathbf{i}} d_{\mathbf{i}}}{\tilde{I}_{\mathbf{i}}}\omega_{\mathbf{i}} v_{x\mathbf{i}}$$
$$\tau_{1\mathbf{i}} = \frac{1}{\tilde{m}_{\mathbf{i}} r_{\mathbf{i}}}(\tau_{L\mathbf{i}} + \tau_{R\mathbf{i}}),\quad \tau_{2\mathbf{i}} = \frac{a_{\mathbf{i}}}{2\tilde{I}_{\mathbf{i}} r_{\mathbf{i}}}(\tau_{R\mathbf{i}} - \tau_{L\mathbf{i}})$$
$$a_{y\mathbf{i}} = d_{\mathbf{i}},\quad a_{\omega\mathbf{i}} = 1$$

where $m_{\mathbf{i}}$, $r_{\mathbf{i}}$ and $a_{\mathbf{i}}$ are mass, wheel radius, and axle length of agent **i**, respectively. $\tilde{m}_{\mathbf{i}} = m_{\mathbf{i}} + 2J_{\mathbf{i}}/r_{\mathbf{i}}^2$, $\tilde{I}_{\mathbf{i}} = I_{\mathbf{i}} + m_{\mathbf{i}} d_{\mathbf{i}}^2 + a_{\mathbf{i}}^2 J_{\mathbf{i}}/r_{\mathbf{i}}^2$, where $I_{\mathbf{i}}$ and $J_{\mathbf{i}}$ are robot and wheel moment of inertia, respectively. $\tau_{L\mathbf{i}}$ and $\tau_{R\mathbf{i}}$ represent the differential torques applied to the left and right wheels, respectively. Note that, the nonholonomic constraint is $v_{y\mathbf{i}} = d_{\mathbf{i}}\omega_{\mathbf{i}}$, where the constant $d_{\mathbf{i}} > 0$ represents the distance from the center of mass of robot **i** to its axle.

Conditions (3) and (4) are satisfied since $\partial f_{y\mathbf{i}}/\partial v_{x\mathbf{i}} = -(m_{\mathbf{i}} d_{\mathbf{i}}^2/\tilde{I}_{\mathbf{i}})\omega_{\mathbf{i}}$, and $\partial f_{y\mathbf{i}}/\partial v_{y\mathbf{i}} = 0$. In this case, $\eta_{\mathbf{i}} = m_{\mathbf{i}} d_{\mathbf{i}}^2/\tilde{I}_{\mathbf{i}}$.

5.2 Surface Vessel With Diagonal Mass Matrix. Comparing the surface vessel **i** model in Ref. [8] with model in Eq. (1), the general terms are derived as

$$f_{x\mathbf{i}} = \frac{m_{22,\mathbf{i}}}{m_{11,\mathbf{i}}} v_{y\mathbf{i}}\omega_{\mathbf{i}} - \frac{d_{11,\mathbf{i}}}{m_{11,\mathbf{i}}}|v_{x\mathbf{i}}|^{\alpha_{11,\mathbf{i}}}\mathrm{sign}(v_{x\mathbf{i}})$$
$$f_{y\mathbf{i}} = -\frac{m_{11,\mathbf{i}}}{m_{22,\mathbf{i}}} v_{x\mathbf{i}}\omega_{\mathbf{i}} - \frac{d_{22,\mathbf{i}}}{m_{22,\mathbf{i}}}|v_{y\mathbf{i}}|^{\alpha_{22,\mathbf{i}}}\mathrm{sign}(v_{y\mathbf{i}})$$
$$f_{\omega\mathbf{i}} = \frac{m_{11,\mathbf{i}} - m_{22,\mathbf{i}}}{m_{33,\mathbf{i}}} v_{x\mathbf{i}} v_{y\mathbf{i}} - \frac{d_{33,\mathbf{i}}}{m_{33,\mathbf{i}}}|\omega_{\mathbf{i}}|^{\alpha_{33,\mathbf{i}}}\mathrm{sign}(\omega_{\mathbf{i}})$$
$$\tau_{1\mathbf{i}} = \frac{F_{\mathbf{i}}}{m_{11,\mathbf{i}}},\ \tau_{2\mathbf{i}} = \frac{T_{\mathbf{i}}}{m_{33,\mathbf{i}}},\ a_{y\mathbf{i}} = 0,\ a_{\omega\mathbf{i}} = 1$$

where the parameters $m_{kk,\mathbf{i}}$'s $(k = 1, 2, 3)$ are positive constants representing the mass and inertia parameters of the surface vessel including the added mass effects. The hydrodynamic damping is represented by the power law parameters $d_{kk,\mathbf{i}}$ and $\alpha_{kk,\mathbf{i}}$, $(k = 1, 2, 3)$. The terms $F_{\mathbf{i}}$ and $T_{\mathbf{i}}$ are the control inputs, which represent the surge force and the yaw moment, respectively. The conditions (3) and (4) in Theorem 1 are satisfied since $\partial f_{y\mathbf{i}}/\partial v_{x\mathbf{i}} = -(m_{11,\mathbf{i}}/m_{22,\mathbf{i}})\omega_{\mathbf{i}}$, and $\partial f_{y\mathbf{i}}/\partial v_{y\mathbf{i}} = -(d_{22,\mathbf{i}}\alpha_{22,\mathbf{i}}/m_{22,\mathbf{i}})|v_{y\mathbf{i}}|^{\alpha_{22,\mathbf{i}}-1} \leq 0$. For this model, $\eta_{\mathbf{i}} = m_{11,\mathbf{i}}/m_{22,\mathbf{i}}$.

5.3 Surface Vessel With Coupled Mass Matrix. In practice, a model including coupling terms in the mass and hydrodynamic damping matrices may be more realistic. Using the model presented in Ref. [8], we can determine the general terms in Eq. (1) for agent **i** as

$$f_{y\mathbf{i}} = a_{\omega\mathbf{i}}\left(f_{y\mathbf{i}'} - \frac{m_{23,\mathbf{i}}}{m_{22,\mathbf{i}}} f_{\omega\mathbf{i}'}\right),\quad \delta_{y\mathbf{i}} = \frac{a_{\omega\mathbf{i}}}{m_{22,\mathbf{i}}}\left(p_{y\mathbf{i}} - \frac{m_{23,\mathbf{i}}}{m_{33,\mathbf{i}}} p_{\omega\mathbf{i}}\right)$$
$$f_{\omega\mathbf{i}} = a_{\omega\mathbf{i}}\left(f_{\omega\mathbf{i}'} - \frac{m_{23,\mathbf{i}}}{m_{33,\mathbf{i}}} f_{y\mathbf{i}'}\right),\quad \delta_{\omega\mathbf{i}} = \frac{a_{\omega\mathbf{i}}}{m_{33,\mathbf{i}}}\left(p_{\omega\mathbf{i}} - \frac{m_{23,\mathbf{i}}}{m_{22,\mathbf{i}}} p_{y\mathbf{i}}\right)$$
$$a_{\omega\mathbf{i}} = \frac{m_{22,\mathbf{i}} m_{33,\mathbf{i}}}{m_{22,\mathbf{i}} m_{33,\mathbf{i}} - m_{23,\mathbf{i}}^2},\quad a_{y\mathbf{i}} = -\frac{m_{23,\mathbf{i}}}{m_{22,\mathbf{i}}} a_{\omega\mathbf{i}}$$
$$f_{x\mathbf{i}'} = \frac{m_{22,\mathbf{i}}}{m_{11,\mathbf{i}}} v_{y\mathbf{i}}\omega_{\mathbf{i}} + \frac{m_{23,\mathbf{i}}}{m_{11,\mathbf{i}}}\omega_{\mathbf{i}}^2 - \frac{d_{11,\mathbf{i}}}{m_{11,\mathbf{i}}} v_{x\mathbf{i}}$$
$$f_{y\mathbf{i}'} = -\frac{m_{11,\mathbf{i}}}{m_{22,\mathbf{i}}} v_{x\mathbf{i}}\omega_{\mathbf{i}} - \frac{d_{22,\mathbf{i}}}{m_{22,\mathbf{i}}} v_{y\mathbf{i}} - \frac{d_{23,\mathbf{i}}}{m_{22,\mathbf{i}}}\omega_{\mathbf{i}}$$
$$f_{\omega\mathbf{i}'} = \frac{m_{11,\mathbf{i}} - m_{22,\mathbf{i}}}{m_{33,\mathbf{i}}} v_{x\mathbf{i}} v_{y\mathbf{i}} - \frac{m_{23,\mathbf{i}}}{m_{33,\mathbf{i}}} v_{x\mathbf{i}}\omega_{\mathbf{i}} - \frac{d_{23,\mathbf{i}}}{m_{33,\mathbf{i}}} v_{y\mathbf{i}} - \frac{d_{33,\mathbf{i}}}{m_{33,\mathbf{i}}}\omega_{\mathbf{i}}$$
$$\tau_{1\mathbf{i}} = \frac{F_{\mathbf{i}}}{m_{11,\mathbf{i}}},\ \tau_{2\mathbf{i}} = \frac{T_{\mathbf{i}}}{m_{33,\mathbf{i}}},\ \delta_{x\mathbf{i}}(t) = \frac{p_{x\mathbf{i}}}{m_{11,\mathbf{i}}}$$

The parameters $m_{23,\mathbf{i}}$, $d_{23,\mathbf{i}}$ are non-negative and represent the off-diagonal terms of the mass and damping matrices, and $p_{x\mathbf{i}}, p_{y\mathbf{i}}, p_{\omega\mathbf{i}}$ consist of environmental disturbances and modeling uncertainties.

Conditions (3) and (4) in Theorem 1 are satisfied if $m_{11,\mathbf{i}} > m_{23,\mathbf{i}}$ and $m_{23,\mathbf{i}}d_{23,\mathbf{i}} < m_{33,\mathbf{i}}d_{22,\mathbf{i}}$ because they guarantee $\eta_{\mathbf{i}} = a_{\omega\mathbf{i}}(m_{11,\mathbf{i}} - m_{23,\mathbf{i}})/(m_{22,\mathbf{i}}) > 0$, and $\partial f_{y\mathbf{i}}/\partial v_{y\mathbf{i}} = a_{\omega\mathbf{i}}(m_{23,\mathbf{i}}d_{23,\mathbf{i}} - m_{33,\mathbf{i}}d_{22,\mathbf{i}})/(m_{22,\mathbf{i}}m_{33,\mathbf{i}}) < 0$. Both of these conditions are inherent to vessel models since the off diagonal terms of the mass and damping matrices are much smaller than the diagonal terms.

5.4 Planar Vertical Takeoff and Landing Aircraft. Consider the model of PVTOL aircraft **i** moving in a vertical plane under the influence of gravity [47]. The general terms introduced in Eq. (1) are

$$f_{x\mathbf{i}} = \omega_{\mathbf{i}} v_{y\mathbf{i}} - g\sin\theta_{\mathbf{i}}, \quad f_{y\mathbf{i}} = -\omega_{\mathbf{i}} v_{x\mathbf{i}} - g\cos\theta_{\mathbf{i}}, \quad f_{\omega\mathbf{i}} = 0$$
$$\tau_{1\mathbf{i}} = \frac{F_{\mathbf{i}}}{m_{\mathbf{i}}}, \quad \tau_{2\mathbf{i}} = \frac{T_{\mathbf{i}}}{I_{\mathbf{i}}}, \quad a_{y\mathbf{i}} = -\frac{\epsilon_{\mathbf{i}} I_{\mathbf{i}}}{m_{\mathbf{i}}}, \quad a_{\omega\mathbf{i}} = 1$$

where $\mathbf{i} = 0, 1, \ldots, N$; $m_{\mathbf{i}}, I_{\mathbf{i}}$ are the mass and the moment of inertia of agent **i**, respectively. The parameter g is the gravity constant and the constant $\epsilon_{\mathbf{i}} > 0$ represents the coupling between the yaw moment and the lateral force on the aircraft.

Conditions (3) and (4) in Theorem 1 are satisfied since $\partial f_{y\mathbf{i}}/\partial v_{x\mathbf{i}} = -\omega_{\mathbf{i}}$, and $\partial f_{y\mathbf{i}}/\partial v_{y\mathbf{i}} = 0$. In this case, $\eta_{\mathbf{i}} = 1$.

6 Numerical Simulations

In this section, two numerical simulations are provided to verify the performance of the proposed formation control approach. All the parameters are given in SI units.

6.1 Example 1. Consider a network of eleven heterogeneous planar underactuated vehicles with the indices $\mathbf{i} = 0, 1, \ldots, 10$. Agent **0** is the leader and agents **1** to **10** are the followers with the communication topology graph as shown in Fig. 3(*a*). Agent **6** and agent **9** have two communication edges such that **6** follows **1** and **5**, and **9** follows **3** and **4**. Note that we assume that the communication from agent **5** to agent **6** is more important than the communication from agent **1** to agent **6**, and that the communication from agent **4** to agent **9** is more important than the communication from agent **3** to agent **9**. Therefore, we set the weighting coefficients $w_{\mathbf{61}} = 0.4$, $w_{\mathbf{65}} = 0.6$, $w_{\mathbf{93}} = 0.3$, $w_{\mathbf{94}} = 0.7$, while the remaining coefficients are all set to 1.

We assume that agents **0** to **3** are identical underactuated surface vessels modeled with diagonal mass matrix and linear hydrodynamic damping ($\alpha_{11,\mathbf{i}} = \alpha_{22,\mathbf{i}} = \alpha_{33,\mathbf{i}} = 1$). The parameters of agents **0** to **3** are given as

$$\begin{aligned} m_{11,\mathbf{i}} &= 1.412, \quad m_{22,\mathbf{i}} = 1.982, \quad m_{33,\mathbf{i}} = 0.354 \\ d_{11,\mathbf{i}} &= 3.436, \quad d_{22,\mathbf{i}} = 12.99, \quad d_{33,\mathbf{i}} = 0.864 \end{aligned} \tag{29}$$

Agents **4** to **6** are also identical underactuated surface vessels modeled with diagonal mass matrix model and nonlinear hydrodynamic damping with the parameters given as

$$\begin{aligned} m_{11,\mathbf{i}} &= 1.317, \quad m_{22,\mathbf{i}} = 3.832, \quad m_{33,\mathbf{i}} = 0.926 \\ d_{11,\mathbf{i}} &= 5.252, \quad d_{22,\mathbf{i}} = 14.138, \quad d_{33,\mathbf{i}} = 2.262 \\ \alpha_{11,\mathbf{i}} &= 1.510, \quad \alpha_{22,\mathbf{i}} = 1.747, \quad \alpha_{33,\mathbf{i}} = 1.592 \end{aligned} \tag{30}$$

Agents **7** to **10** are identical nonholonomic mobile robots with the parameters given as

$$\begin{aligned} m_{\mathbf{i}} &= 3.0, \quad I_{\mathbf{i}} = 0.025, \quad J_{\mathbf{i}} = 6 \times 10^{-6} \\ a_{\mathbf{i}} &= 0.33, \quad d_{\mathbf{i}} = 0.08, \quad r_{\mathbf{i}} = 0.05 \end{aligned} \tag{31}$$

In this simulation, the leader is commanded to follow a straight line in the x-direction with desired velocity 1 m/s. The geometric shape of the desired formation for the ten follower vehicles is a pentagram, where the center of the pentagram is located at the leader. Then, the positions of the ten follower agents are to be driven to the ten vertices of the pentagram, as shown in Fig. 3(*a*). The radius of the circumscribed circle of the inner five vertices is set to 3 m, and the corresponding radius of the circumscribed circle of the outer five vertices is 9.434 m. The pentagram rotates counterclockwise around its center with a constant angular velocity of 0.5 rad/s, making the formation time-varying. All vehicles start from rest at zero orientation, while their initial positions can be observed in Fig. 4.

To demonstrate robustness, we applied disturbances $\delta_{x\mathbf{i}}(t) = 0.25\sin(t) + 0.5\sin(20t)$ and $\delta_{\omega\mathbf{i}}(t) = 0.4\sin(t) + 0.5\sin(10t)$. We also assume that the communication between agents **5** and **6**, and the communication between agents **4** and **9** suddenly breaks at $t = 5$ s. The control gains and disturbance bounds for all agents were selected as $\lambda_1 = \lambda_2 = \lambda_3 = -1, k_{1\mathbf{i}} = k_{2\mathbf{i}} = c_{\mathbf{i}} = 3$, $\Delta_{x\mathbf{i}} = \Delta_{\omega\mathbf{i}} = 0.75$, $\mathbf{i} = 1, \ldots, 10$. To avoid excessive chattering, we used the hyperbolic tangent function $\tanh(\cdot/0.01)$ to approximate the discontinuous signum function .

Figure 4 illustrates the position trajectories of all agents at $t = 0$ s, $t = 25$ s, and $t = 45$ s. It is clear that the desired pentagram formation is achieved after the leader has traveled approximately 25 m in just over 25 s. Figure 5 shows the time history of the root mean squared of all formation errors, which is of the form $\mathrm{RMS}([\cdot]_{\mathbf{i}}) = (\frac{1}{n}\sum_{i=1}^{n}([\cdot] - [\cdot]_{\mathbf{i}})^2)^{1/2}$, demonstrating formation converging after 25 s. It can also be seen that the breakage of communication at $t = 5$ s temporarily increases the overall formation errors but the asymptotic convergence continues after a short interruption.

6.2 Example 2. Consider a network of six heterogeneous planar underactuated vehicles with the indices $\mathbf{i} = 0, 1, \ldots, 5$. Agent **0** is the leader and agents **1** to **5** are the followers with the

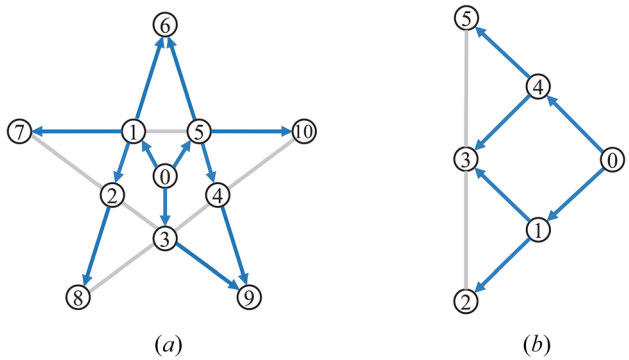

Fig. 3 Communication topology graphs in the simulations: (*a*) Example 1 and (*b*) Example 2

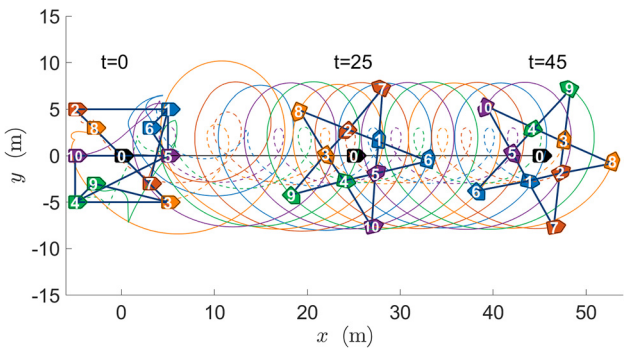

Fig. 4 Illustration of the trajectories of the eleven planar vehicles in Example 1

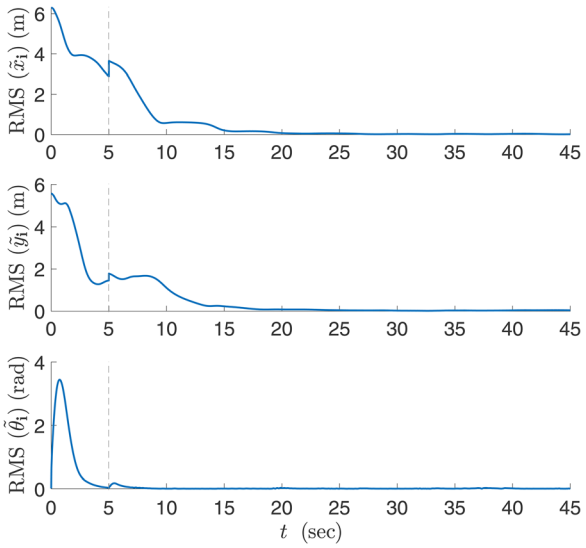

Fig. 5 Convergence of the RMS formation errors of the ten follower vehicles in Example 1

communication topology graph as shown in Fig. 3(*b*). We set the weighting coefficients $w_{31} = w_{34} = 0.5$ while the remaining coefficients are all set to 1.

Agent **0** is a PVTOL aircraft, where the model parameters are given as $m_i = 1$, $I_i = 0.1, \epsilon_i = 0.2$, and $g = 9.81$. Agents **1** and **2** are wheeled mobile robots, where the model parameters are given as (31). Agents **3** to **5** are different surface vessels, where agent **3** is with linear hydrodynamic damping, and the model parameters are given as Eq. (29); agents **4** and **5** are with nonlinear hydrodynamic damping and the model parameters are given as Eq. (30). We use the scenario where all types of vehicles are involved in coordination in order to show the versatility of the approach.

In this simulation, the leader is commanded to follow a sinusoidal path, i.e., $(x_d(t), y_d(t)) = (t, \sin(t))$. The geometric shape of the desired formation for the six vehicles is an time-varying isosceles right triangle, as shown in Fig. 3(*b*). We set the length of the two congruent sides to $\sqrt{2}(20 - t/6)$. In other words, the position offsets are given as $(d^x_{40}, d^y_{40}) = (d^x_{54}, d^y_{54}) = (t/12 - 10, 10 - t/12)$, $(d^x_{10}, d^y_{10}) = (d^x_{21}, d^y_{21}) = (d^x_{34}, d^y_{34}) = (t/12 - 10, t/12 - 10)$. All vehicles start from rest at zero orientation, while their initial positions can be observed in Fig. 6.

To demonstrate robustness, we applied disturbances $\delta_{xi}(t) = 0.25\sin(t) + 0.5\sin(20t)$ and $\delta_{\omega i}(t) = 0.4\sin(t) + 0.5\sin(10t)$.

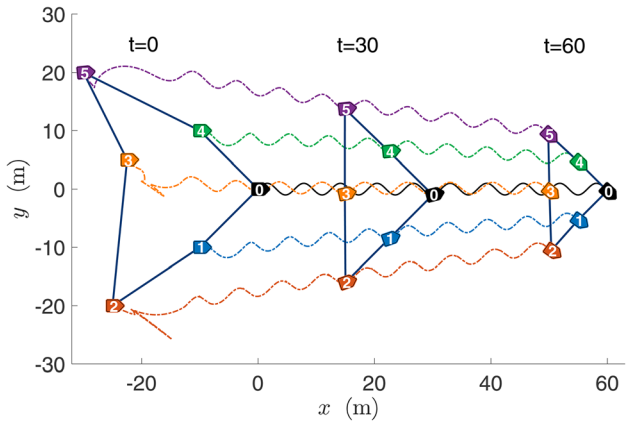

Fig. 6 Illustration of the trajectories of the six planar vehicles in Example 2

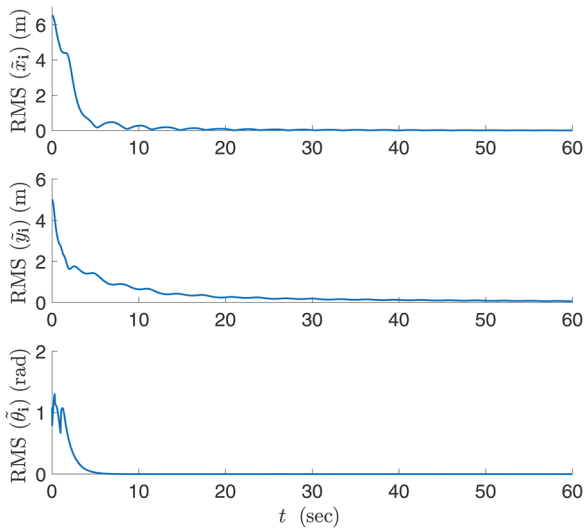

Fig. 7 Convergence of the RMS formation errors of the six follower vehicles in Example 2

The control gains and disturbance bounds for all agents were selected as $\lambda_1 = \lambda_2 = \lambda_3 = -1, k_{1i} = k_{2i} = c_i = 5, \Delta_{xi} = \Delta_{\omega i} = 0.75$, $i = 1, \ldots, 5$. Figure 6 illustrates the position trajectories of all agents at $t = 0$ s, $t = 30$ s, and $t = 60$ s. Note that when the angular velocity $\omega_i(t) = 0$, the hybrid control law is used to avoid singularity as discussed in Remark 3. It is clear that the desired triangle formation is achieved after the leader has traveled approximately 30 m in just over 30 s. Figure 7 shows the time history of the RMS formation errors demonstrating formation converging after about 30 s.

7 Conclusion

In this work, we develop a distributed formation control approach for networks of *heterogeneous* planar *underactuated* vehicles *without requiring global position measurements*. All vehicles in the network are modeled as generic three degree-of-freedom planar rigid bodies with two control inputs, and are allowed to have nonidentical dynamics. The feasible trajectory for each vehicle in the network is generated based on the nonholonomic constraint of the vehicle. A transformation is proposed to reduce the order of error dynamics and then a sliding mode control law is employed to stabilize the error dynamics. While the sliding mode control approach is selected, other methods such as backstepping technique can also be employed using the same error transformation introduced in this work. It is shown that the approach can be applied to networks of nonholonomic mobile robots, underactuated surface vessels with various modeling complexities, and planar air vehicles. We successfully apply the proposed approach to a time-varying formation control problem for a complex network of heterogeneous mobile robots and surface vessels. Our future research will focus on multivehicle formation control with saturation constraints, and formation control of heterogeneous three-dimensional underactuated vehicle networks.

Appendix: Force–Balance Equations

Wheeled mobile robots. The force–balance equations for mobile robot **i** (Fig. 8(*a*)) with nonholonomic constraint $v_{yi} = d_i\omega_i$ are given by [24]

$$\dot{v}_{xi} = \frac{m_i d_i}{\tilde{m}_i}\omega_i^2 + \frac{1}{\tilde{m}_i r_i}(\tau_{Li} + \tau_{Ri}) + \delta_{xi}(t)$$

$$\dot{\omega}_i = -\frac{m_i d_i}{\tilde{I}_i}\omega_i v_{xi} + \frac{a_i}{2\tilde{I}_i r_i}(\tau_{Ri} - \tau_{Li}) + \delta_{\omega i}(t)$$

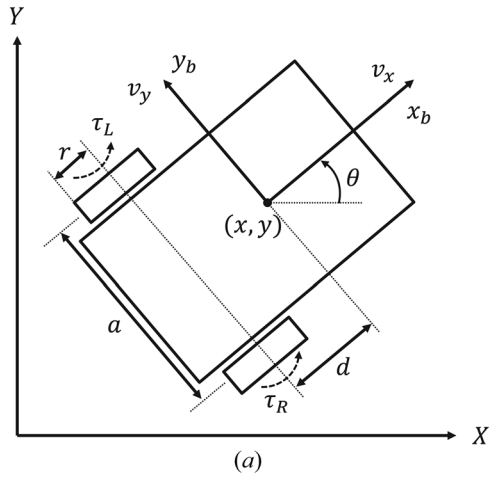

(a)

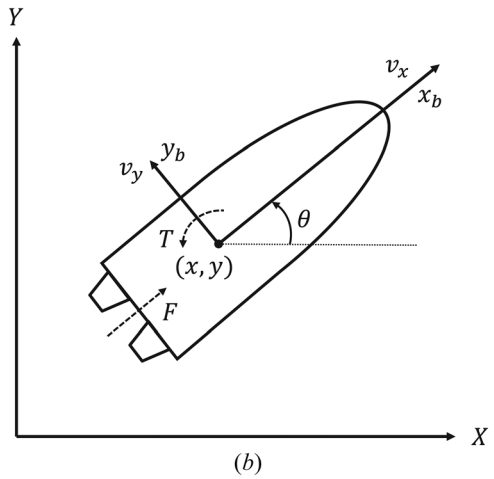

(b)

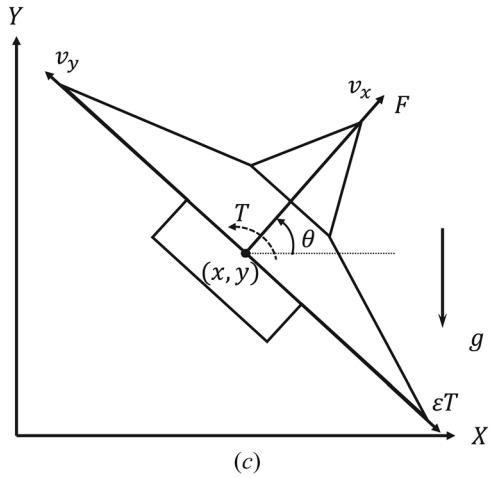

(c)

Fig. 8 Underactuated planar vehicle models: (*a*) nonholonomic mobile robot, (*b*) marine surface vessel, and (*c*) PVTOL aircraft

Surface vessel with diagonal mass matrix. The force–balance equations of a underactuated surface vessel **i** (Fig. 8(*b*)) model with nonlinear hydrodynamic damping are given by [8]

$$\dot{v}_{x\mathbf{i}} = \frac{m_{22,\mathbf{i}}}{m_{11,\mathbf{i}}} v_{y\mathbf{i}}\omega_{\mathbf{i}} - \frac{d_{11,\mathbf{i}}}{m_{11,\mathbf{i}}}|v_{x\mathbf{i}}|^{\alpha_{11,\mathbf{i}}}\text{sign}(v_{x\mathbf{i}}) + \frac{F_{\mathbf{i}}}{m_{11,\mathbf{i}}} + \delta_{x\mathbf{i}}(t)$$

$$\dot{v}_{y\mathbf{i}} = -\frac{m_{11,\mathbf{i}}}{m_{22,\mathbf{i}}} v_{x\mathbf{i}}\omega_{\mathbf{i}} - \frac{d_{22,\mathbf{i}}}{m_{22,\mathbf{i}}}|v_{y\mathbf{i}}|^{\alpha_{22,\mathbf{i}}}\text{sign}(v_{y\mathbf{i}}) + \delta_{y\mathbf{i}}(t)$$

$$\dot{\omega}_{\mathbf{i}} = \frac{m_{d,\mathbf{i}}}{m_{33,\mathbf{i}}} v_{x\mathbf{i}}v_{y\mathbf{i}} - \frac{d_{33,\mathbf{i}}}{m_{33,\mathbf{i}}}|\omega_{\mathbf{i}}|^{\alpha_{33,\mathbf{i}}}\text{sign}(\omega_{\mathbf{i}}) + \frac{T_{\mathbf{i}}}{m_{33,\mathbf{i}}} + \delta_{\omega\mathbf{i}}(t)$$

This model is also applicable to linear hydrodynamic damping with $\alpha_{11,\mathbf{i}} = \alpha_{22,\mathbf{i}} = \alpha_{22,\mathbf{i}} = 1$.

Surface vessel with coupled mass matrix. The force–balance equations of a underactuated surface vessel **i** (Fig. 8(*b*)) model with couple mass matrix are given by [8]

$$\begin{bmatrix} m_{11,\mathbf{i}} & 0 & 0 \\ 0 & m_{22,\mathbf{i}} & m_{23,\mathbf{i}} \\ 0 & m_{23,\mathbf{i}} & m_{33,\mathbf{i}} \end{bmatrix} \begin{bmatrix} \dot{v}_{x\mathbf{i}} \\ \dot{v}_{y\mathbf{i}} \\ \dot{\omega}_{\mathbf{i}} \end{bmatrix} + \begin{bmatrix} -m_{22,\mathbf{i}}v_{y\mathbf{i}}\omega_{\mathbf{i}} - m_{23,\mathbf{i}}\omega_{\mathbf{i}}^2 \\ m_{11,\mathbf{i}}v_{x\mathbf{i}}\omega_{\mathbf{i}} \\ -m_{d,\mathbf{i}}v_{x\mathbf{i}}v_{y\mathbf{i}} + m_{23,\mathbf{i}}v_{x\mathbf{i}}\omega_{\mathbf{i}} \end{bmatrix} + \begin{bmatrix} d_{11,\mathbf{i}} & 0 & 0 \\ 0 & d_{22,\mathbf{i}} & d_{23,\mathbf{i}} \\ 0 & d_{23,\mathbf{i}} & d_{33,\mathbf{i}} \end{bmatrix} \begin{bmatrix} v_{x\mathbf{i}} \\ v_{y\mathbf{i}} \\ \omega_{\mathbf{i}} \end{bmatrix} = \begin{bmatrix} F_{\mathbf{i}} \\ 0 \\ T_{\mathbf{i}} \end{bmatrix}$$

PVTOL aircraft. The force–balance equations for PVTOL aircraft **i** (Fig. 8(*c*)) controlled by the force $F_{\mathbf{i}}$ and moment $T_{\mathbf{i}}$ is given as [47]

$$\ddot{x} = \frac{F_{\mathbf{i}}}{m_{\mathbf{i}}}\cos\theta_{\mathbf{i}} + \frac{\epsilon_{\mathbf{i}}T_{\mathbf{i}}}{m_{\mathbf{i}}}\sin\theta_{\mathbf{i}}$$

$$\ddot{y} = \frac{F_{\mathbf{i}}}{m_{\mathbf{i}}}\sin\theta_{\mathbf{i}} - \frac{\epsilon_{\mathbf{i}}T_{\mathbf{i}}}{m_{\mathbf{i}}}\cos\theta_{\mathbf{i}} - g$$

$$\ddot{\theta} = \frac{T_{\mathbf{i}}}{I_{\mathbf{i}}}$$

After some manipulation and inclusion of uncertainties, the equations in form (1) are given by

$$\dot{v}_{x\mathbf{i}} = \omega_{\mathbf{i}}v_{y\mathbf{i}} - g\sin\theta_{\mathbf{i}} + \frac{F_{\mathbf{i}}}{m_{\mathbf{i}}} + \delta_{x\mathbf{i}}(t)$$

$$\dot{v}_{y\mathbf{i}} = -\omega_{\mathbf{i}}v_{x\mathbf{i}} - g\cos\theta_{\mathbf{i}} - \frac{\varepsilon_{\mathbf{i}}T_{\mathbf{i}}}{m_{\mathbf{i}}} + \delta_{y\mathbf{i}}(t)$$

$$\dot{\omega}_{\mathbf{i}} = \frac{T_{\mathbf{i}}}{I_{\mathbf{i}}} + \delta_{\omega\mathbf{i}}(t)$$

Funding Data

- U.S. Office of Naval Research (Grant No. N00014-19-1-2255; Funder ID: 10.13039/100000006).

References

[1] Canudas-de Wit, C., Khennouf, H., Samson, C., and Sordalen, O. J., 1993, "Nonlinear Control Design for Mobile Robots," *Recent Trends in Mobile Robots*, Y. F. Zheng, ed., Vol. 11, World Scientific Series in Robotics and Intelligent Systems, River Edge, NJ, pp. 121–156.

[2] Panteley, E., Lefeber, E., Loria, A., and Nijmeijer, H., 1998, "Exponential Tracking Control of a Mobile Car Using a Cascaded Approach," IFAC Proc. Vols., **31**(27), pp. 201–206.

[3] Wang, B., Ashrafiuon, H., and Nersesov, S. G., 2021, "The Use of Partial Stability in the Analysis of Interconnected Systems," ASME J. Dyn. Syst. Meas. Control, **143**(4), p. 044501.

[4] Do, K. D., Jiang, Z.-P., and Pan, J., 2002, "Underactuated Ship Global Tracking Under Relaxed Conditions," IEEE Trans. Autom. Control, **47**(9), pp. 1529–1536.

[5] Jiang, Z.-P., 2002, "Global Tracking Control of Underactuated Ships by Lyapunov's Direct Method," Automatica, **38**(2), pp. 301–309.

[6] Yu-Chan, C., Bao-Li, M., and Wen-Jing, X., 2017, "Robust Stabilization of Nonlinear PVTOL Aircraft With Parameter Uncertainties," Asian J. Control, **19**(3), pp. 1239–1249.

[7] Consolini, L., Maggiore, M., Nielsen, C., and Tosques, M., 2010, "Path Following for the PVTOL Aircraft," Automatica, **46**(8), pp. 1284–1296.

[8] Ashrafiuon, H., Nersesov, S., and Clayton, G., 2017, "Trajectory Tracking Control of Planar Underactuated Vehicles," IEEE Trans. Autom. Control, **62**(4), pp. 1959–1965.

[9] Ren, W., and Cao, Y., 2010, *Distributed Coordination of Multi-Agent Networks: Emergent Problems, Models, and Issues*, Springer-Verlag, London, UK.

[10] Consolini, L., Morbidi, F., Prattichizzo, D., and Tosques, M., 2008, "Leader–Follower Formation Control of Nonholonomic Mobile Robots With Input Constraints," Automatica, **44**(5), pp. 1343–1349.

[11] Egerstedt, M., and Hu, X., 2001, "Formation Constrained Multi-Agent Control," IEEE Trans. Robot. Automat., **17**(6), pp. 947–951.
[12] Tabuada, P., Pap, G. J., and Lima, P., 2005, "Motion Feasibility of Multi-Agent Formations," IEEE Trans. Robot., **21**(3), pp. 387–392.
[13] Ren, W., and Beard, R. W., 2005, "Consensus Seeking in Multiagent Systems Under Dynamically Changing Interaction Topologies," IEEE Trans. Autom. Control, **50**(5), pp. 655–661.
[14] Ren, W., 2008, "On Consensus Algorithms for Double-Integrator Dynamics," IEEE Trans. Autom. Control, **53**(6), pp. 1503–1509.
[15] Antonelli, G., Arrichiello, F., Caccavale, F., and Marino, A., 2014, "Decentralized Time-Varying Formation Control for Multi-Robot Systems," Int. J. Rob. Res., **33**(7), pp. 1029–1043.
[16] Seo, J. H., Shim, H., and Back, J., 2009, "Consensus of High-Order Linear Systems Using Dynamic Output Feedback Compensator: Low Gain Approach," Automatica, **45**(11), pp. 2659–2664.
[17] Ren, W., 2006, "Distributed Attitude Consensus Among Multiple Networked Spacecraft," Proceedings of American Control Conference, IEEE, Minneapolis, MN, June 14–16, pp. 4237–4242.
[18] Dimarogonas, D. V., Tsiotras, P., and Kyriakopoulos, K. J., 2009, "Leader–Follower Cooperative Attitude Control of Multiple Rigid Bodies," Sys. Contr. Lett., **58**(6), pp. 429–435.
[19] Mei, J., Ren, W., and Ma, G., 2011, "Distributed Coordinated Tracking With a Dynamic Leader for Multiple Euler-Lagrange Systems," IEEE Trans. Autom. Control, **56**(6), pp. 1415–1421.
[20] Das, A. K., Fierro, R., Kumar, V., Ostrowski, J. P., Spletzer, J., and Taylor, C. J., 2002, "A Vision-Based Formation Control Framework," IEEE Trans. Robot. Autom., **18**(5), pp. 813–825.
[21] Dong, W., and Farrell, J. A., 2008, "Cooperative Control of Multiple Nonholonomic Mobile Agents," IEEE Trans. Autom. Control, **53**(6), pp. 1434–1448.
[22] Yan, L., and Ma, B., 2020, "Adaptive Practical Leader-Following Formation Control of Multiple Nonholonomic Wheeled Mobile Robots," Int. J. Robust Nonlinear Control, **30**(17), pp. 7216–7237.
[23] Liu, T., and Jiang, Z.-P., 2013, "Distributed Formation Control of Nonholonomic Mobile Robots Without Global Position Measurements," Automatica, **49**(2), pp. 592–600.
[24] Ghasemi, M., Nersesov, S. G., Clayton, G., and Ashrafiuon, H., 2014, "Sliding Mode Coordination Control for Multiagent Systems With Underactuated Agent Dynamics," Int. J. Control, **87**(12), pp. 2615–2633.
[25] Kamel, M. A., Yu, X., and Zhang, Y., 2020, "Real-Time Fault-Tolerant Formation Control of Multiple WMRS Based on Hybrid GA-PSO Algorithm," IEEE Trans. Autom. Sci. Eng., **18**, pp. 1263–1276.
[26] Kamel, M. A., Yu, X., and Zhang, Y., 2020, "Formation Control and Coordination of Multiple Unmanned Ground Vehicles in Normal and Faulty Situations: A Review," Annu. Rev. Control, **49**, pp. 128–144.
[27] Dong, W., and Farrell, J., 2008, "Formation Control of Multiple Underactuated Surface Vessels," IET Control Theory Appl., **2**(12), pp. 1077–1085.
[28] Dong, W., 2010, "Cooperative Control of Underactuated Surface Vessels," IET Control Theory Appl., **4**(9), pp. 1569–1580.
[29] Jin, X., 2016, "Fault Tolerant Finite-Time Leader–Follower Formation Control for Autonomous Surface Vessels With LOS Range and Angle Constraints," Automatica, **68**, pp. 228–236.
[30] Do, K. D., 2015, "Coordination Control of Quadrotor VTOL Aircraft in Three-Dimensional Space," Int. J. Control, **88**(3), pp. 543–558.
[31] Liao, F., Teo, R., Wang, J. L., Dong, X., Lin, F., and Peng, K., 2017, "Distributed Formation and Reconfiguration Control of VTOL UAVs," IEEE Trans. Control Syst. Technol., **25**(1), pp. 270–277.
[32] Yu, X., Liu, Z., and Zhang, Y., 2016, "Fault-Tolerant Formation Control of Multiple Uavs in the Presence of Actuator Faults," Int. J. Robust Nonlinear Control, **26**(12), pp. 2668–2685.
[33] Valk, L., 2018, "Distributed Control of Underactuated and Heterogeneous Mechanical Systems," Master's thesis, Delft University of Technology, Delft, The Netherlands.
[34] Wang, B., Nersesov, S., and Ashrafiuon, H., 2020, "A Unified Approach to Stabilization, Trajectory Tracking, and Formation Control of Planar Underactuated Vehicles," Proceedings of American Control Conference, IEEE, Denver, CO, July 1–3, pp. 5269–5274.
[35] Oh, K.-K., Park, M.-C., and Ahn, H.-S., 2015, "A Survey of Multi-Agent Formation Control," Automatica, **53**, pp. 424–440.
[36] Oh, K.-K., and Ahn, H.-S., 2011, "Formation Control of Mobile Agents Based on Inter-Agent Distance Dynamics," Automatica, **47**(10), pp. 2306–2312.
[37] Wang, B., Nersesov, S., and Ashrafiuon, H., 2020, "Formation Control for Underactuated Surface Vessel Networks," ASME Paper No. DSCC2020-3178.
[38] Mesbahi, M., and Egerstedt, M., 2010, *Graph Theoretic Methods in Multiagent Networks*, Princeton University Press, Princeton, NJ.
[39] Desoer, C. A., and Vidyasagar, M., 1975, *Feedback Systems: Input-Output Properties*, Siam, Philadelphia, PA.
[40] Panteley, E., Loria, A., and Teel, A., 2001, "Relaxed Persistency of Excitation for Uniform Asymptotic Stability," IEEE Trans. Autom. Control, **46**(12), pp. 1874–1886.
[41] Khalil, H. K., 2002, *Nonlinear Systems*, 3rd ed., Prentice Hall, Englewood Cliffs, NJ.
[42] Yang, J., Chen, W.-H., and Li, S., 2011, "Non-Linear Disturbance Observer-Based Robust Control for Systems With Mismatched Disturbances/Uncertainties," IET Control Theory Appl., **5**(18), pp. 2053–2062.
[43] Guo, L., and Chen, W.-H., 2005, "Disturbance Attenuation and Rejection for Systems With Nonlinearity Via Dobc Approach," Int. J. Robust Nonlinear Control, **15**(3), pp. 109–125.
[44] Yang, J., Li, S., and Yu, X., 2013, "Sliding-Mode Control for Systems With Mismatched Uncertainties Via a Disturbance Observer," IEEE Trans. Ind. Electron., **60**(1), pp. 160–169.
[45] Cruz-Zavala, E., Moreno, J. A., and Fridman, L. M., 2011, "Uniform Robust Exact Differentiator," IEEE Trans. Autom. Control, **56**(11), pp. 2727–2733.
[46] Vasiljevic, L. K., and Khalil, H. K., 2008, "Error Bounds in Differentiation of Noisy Signals by High-Gain Observers," Syst. Control Lett., **57**(10), pp. 856–862.
[47] Sastry, S., 2013, *Nonlinear Systems: Analysis, Stability, and Control*, Springer, New York.